JOURNAL OF PROPULSION AND POWER
Vol. 25, No. 2, March–April 2009

Influence of Heat Capacity Ratio on Pressure and Nozzle Flow of Scramjets

C. Hirschen* and A. Gülhan†
DLR, German Aerospace Center, 51147 Cologne, Germany

DOI: 10.2514/1.39380

An experimental study of flows over a single expansion ramp nozzle with side walls was carried out at the German Aerospace Center (DLR). The tests were performed at a freestream Mach number of 7 in the hypersonic wind tunnel H2K of the wind-tunnel department in Cologne. The Reynolds number, nozzle pressure ratio, and the heat capacity ratio were varied in order to study the performance of the scramjet nozzle at different flight altitudes and run conditions. The effects of different heat capacity ratios have been investigated by using gases with higher and lower heat capacity ratios than air. The static pressure distribution on the single expansion ramp was measured by using Pressure System Incorporated pressure transducer taps located at discrete points on the surface. Schlieren photographs were taken by a high-speed camera to visualize the flowfield and investigate the influence of the heat capacity ratio on the interactions between the external and the nozzle flow. The obtained experimental results are discussed and compared with the Schlieren photographs. An effect of the heat capacity ratio on the pressure distribution and the interactions between external and nozzle flow was found. The data obtained by the different measurement techniques permitted a characterization of the nozzle flow and gave insight into the properties of single expansion ramp nozzle flows.

Nomenclature

A	=	area, m^2
Ma	=	Mach number, −
p	=	pressure, $N \cdot m^2$
R	=	specific gas constant, for air $R = 287.15$, $J \cdot kg^{-1} \cdot K^{-1}$
Re_U	=	unit Reynolds number, m^{-1}
T	=	temperature, K
x	=	streamwise distance from nozzle entry, mm
y	=	spanwise direction from nozzle centerline, mm
z	=	height above or below flap (see Fig. 4), mm
γ	=	heat capacity ratio, −
Δp_0	=	pressure loss, −, $\Delta p_0 = 1 - p_{02}/p_{01}$
δ	=	deflection angle, deg
Π	=	nozzle pressure ratio, −, $\Pi = p_{0,N}/p_\infty$
ρ	=	density, $kg \cdot m^{-3}$
σ	=	oblique shock wave angle, deg

Subscripts

E	=	exit
N	=	nozzle conditions
0	=	total conditions
1	=	conditions in front of the shock
2	=	conditions behind the shock
∞	=	wind-tunnel freestream conditions

I. Introduction

TO SAVE weight and increase the maximum payload of space transportation systems, airbreathing propulsion is an alternative to the existing rocket propulsion systems which carry their oxidant (e.g., liquid oxygen) on board [1–3]. Aerodynamic stability and generation of sufficient thrust are major problems of a hypersonic vehicle with scramjet propulsion, whereby the nozzle and external base flow interactions play a large role [4]. Although the interaction of the hypersonic nozzle/afterbody flowfield with a cold plume flow has been extensively studied [5–7], there is still a lack of experimental data. It is therefore necessary to study the aerodynamic phenomena which arise from the interaction between the external base flow and the hot nozzle flow, and to understand their effects on the nozzle performance. This interaction is mainly driven by temperature, viscosity, and heat capacity ratio effects.

The dynamic interactions between the aerodynamics of the vehicle and the thrust have also been studied numerically [8,9]. Ebrahimi [10] introduced an efficient design code for scramjet nozzle design. Ishiguro et al. in [11] show the results of a three-dimensional analysis of scramjet nozzle flows which agree well in certain aspects with the experimental results. In [12] the effects on the flow interaction of employing simulant gases instead of air for the scramjet nozzle flow are presented. Experimental studies investigating the interactions between the external flow and internal nozzle flow have been shown to be very complex and not fully understood as yet [13–15]. In [16] a broad experimental study on the boundary-layer effects in a scramjet nozzle has been carried out. These experimental and numerical studies, however, point to the necessity of further research in this field.

As part of a research project that aims to improve the key technologies for the design of a scramjet propulsion unit [17], it is the goal of this study to investigate the flow of a scramjet nozzle and carry out an experimental study of its performance. Mitani et al. [18] performed an experimental study on the performance of a scramjet nozzle, where they compared the experimental data with the results obtained by an inviscid two-dimensional chemical kinetic code. They showed that lift thrust and main thrust are comparable and very sensitive to the nozzle configuration.

One of the objectives of this study is to gain information about the influence and effects of the heat capacity ratio γ on the aerodynamics of the nozzle flow. The main goal of this experimental study is to study these effects separately from the influence of the temperature. Normally, the heat capacity ratio of air decreases with increasing temperature. In this case, however, the viscosity of air also increases and influences the nozzle flow and the interactions. So it is difficult to distinguish between the influence of a decreasing heat capacity ratio

Presented as Paper 8095 at the 14th AIAA/AHI Space Planes and Hypersonic Systems and Technologies Conference, Canberra, Australia, 6–9 November 2006; received 26 June 2008; accepted for publication 8 December 2008.

*Ph.D. Student, Wind Tunnel Department, Institute of Aerodynamics and Flow Technology, Linder Höhe. Student Member AIAA.

†Head of Department, Wind Tunnel Department, Institute of Aerodynamics and Flow Technology, Linder Höhe. Member AIAA.

and increasing viscosity, if they both change at the same time. Therefore, an experimental study with three gases with different heat capacity ratios was performed at ambient temperature conditions. This allows the investigation of the effects of the heat capacity ratio to be separated from the effects of the temperature. The gases used are air, sulfur hexafluoride (SF6), and argon, whereas argon has a higher heat capacity ratio ($\gamma = 1.667$) and SF6 a lower ($\gamma = 1.1$) heat capacity ratio than air. This test procedure allows the analysis of the behavior of air as the nozzle fluid at higher temperatures in combination with lower heat capacity ratio. Pressure measurements and Schlieren photographs give a first idea of the effects and impacts caused by different heat capacity ratios. Furthermore, the influence of the heat capacity ratio on the topology of a single expansion ramp nozzle flow and its aerodynamic interactions with the external base flow were investigated. It is also important to measure the pressure distribution along the single expansion ramp for different gases, because the heat capacity ratio of the flow generated by the combustion in the scramjet is lower than the one of air. For the design process of the single expansion ramp, the thrust has to be predicted as exact as possible and must not be under- or overestimated [12,19]. The use of stimulant gas with a heat capacity ratio close to the one of the real scramjet engine is helpful to estimate the correct pressure distribution and gross thrust.

Finally, the nozzle pressure ratio Π and the Reynolds number Re_U were varied to study their influence during different flight conditions. These experiments were performed at a freestream Mach number $Ma_\infty = 7$ and a Reynolds number range from $Re_U = 4 \times 10^6$ to $Re_U = 8 \times 10^6$, corresponding to different flight altitudes of 30 and 25 km, respectively. According to former experimental studies, the nozzle pressure ratio Π and the freestream Reynolds number Re_U are the main parameters affecting the nozzle flow behavior [20]. The nozzle pressure ratio Π was varied to study its influence on the shock and shear layer positions, the exhaust plume shape, the pressure distributions, and the gross thrust. Therefore, different measurement techniques were applied and the results compared with each other. The different measurement techniques enabled the visualization of different flow aspects such as shock positions, shear layer position, surface pressure distribution, and exhaust plume shape. Shock and shear layer position as well as the shape of the exhaust plume were measured and visualized by means of Schlieren photographs. The surface pressure distribution was obtained by pressure static measurements (using embedded sensors).

II. Experimental Methods

A. Wind Tunnel and Test Conditions

The experiments were carried out in the German Aerospace Center (DLR) hypersonic wind-tunnel facility H2K in Cologne, which has been described in more detail elsewhere [21]. This facility is a blowdown wind tunnel with test durations of up to 30 s, depending on the flow conditions. The facility is equipped with five contoured nozzles with varying throat diameters and a constant exit diameter of 600 mm, leading to flow Mach numbers of $Ma_\infty = 5.3, 6, 7, 8.7$, and 11.2. For these experiments, the Mach 7 nozzle was used. Dried air passes from a pressure reservoir with a maximum pressure of 4.5 MPa through electrical heaters with a heating power of 5 MW, thereby heating the air to temperatures of up to 1000 K; this avoids later potential condensation effects in the nozzle expansion. The operational range of the H2K wind tunnel can be seen in Fig. 1a, where the performance map with respect to the Mach number and unit Reynolds number Re_U is depicted, with total pressure p_0 and mass flow rate $\dot{m}$ as parameters. The solid black vertical lines pertain to the available wind-tunnel nozzles. The unit Reynolds number is given by the proper choice of the reservoir pressure p_0 and the total temperature T_0 of the flow. A schematic sketch of the hypersonic wind-tunnel facility is shown in Fig. 1b.

The wind-tunnel flow conditions for these tests with the nozzle model are summarized in Table 1; the accuracy of measurement is as follows: $\Delta Ma/Ma = 0.5\%$, $\Delta T_0/T_0 = 0.75\%$, and $\Delta p_0/p_0 = 0.02\%$.

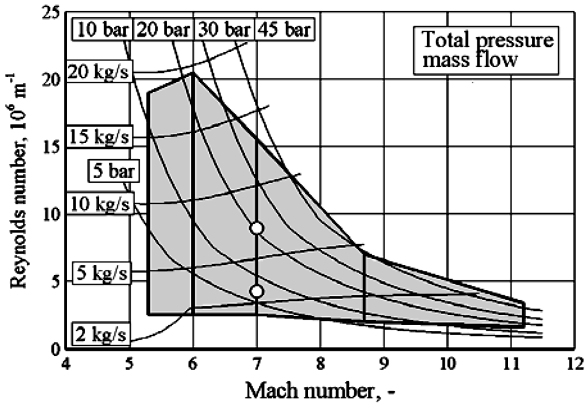

a) Performance map

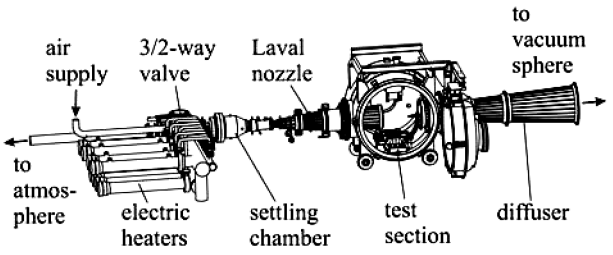

b) Schematic sketch

Fig. 1 Hypersonic wind-tunnel facility H2K.

B. Model

For the simulation and investigation of the interaction between the nozzle flow and external base flow, an experimental wind-tunnel model was used which consists of two main parts: forebody and nozzle (see Fig. 2). The single expansion ramp nozzle (SERN) has a three-dimensional geometry as can be seen in the picture. The forebody was designed to fit onto the existing single expansion ramp nozzle (Fig. 2a) and to supply this nozzle with its own (exhaust) gas flow; in these experiments this gas was not heated. During these tests the model and tunnel axes were aligned in parallel. The exhaust gas was supplied to the nozzle plenum by a pipe, which was mounted on the side of the forebody at one end and connected to a tube at the other end. Through this connecting tube the different gases, which are stored in external separate reservoirs near the wind tunnel, were injected into the model plenum. To provide a uniform flow, a honeycomb followed by a contoured 2-D Laval nozzle (Fig. 2a) were installed inside the forebody. The Laval nozzle was necessary to provide supersonic flow, because single expansion ramp nozzles of scramjet engines do not have a sonic throat. The inserted Laval nozzle elements can be replaced to simulate different Mach numbers at the combustor exit; for these experiments the Mach number nozzle entrance is $Ma = 2$. The entrance to the single expansion ramp nozzle has a cross-sectional area of 19 mm height × 60 mm width.

The model is a 3-D single expansion ramp nozzle (see Fig. 3) with a total length of 214 mm and a total height of 101 mm. This nozzle was originally designed in the framework of the Joint Airbreathing Propulsion for Hypersonic Application Research (JAPHAR) program [22]. The nozzle is equipped with 51 pressure taps (orifices) in total with a diameter of 0.5 mm. There are four on the cowl, three on the side, and 44 on the single expansion ramp, being

Table 1 Wind-tunnel flow conditions

Freestream Mach number Ma_∞, –	7	7
Freestream pressure p_∞, Pa	260	515
Freestream temperature T_∞, K	60	60
Freestream density ρ_∞, kg/m^3	0.015	0.029
Total temperature T_0, K	650	650
Total pressure p_0, Pa	10×10^5	21×10^5
Unit Reynolds number Re_U, –	4×10^6	8×10^6

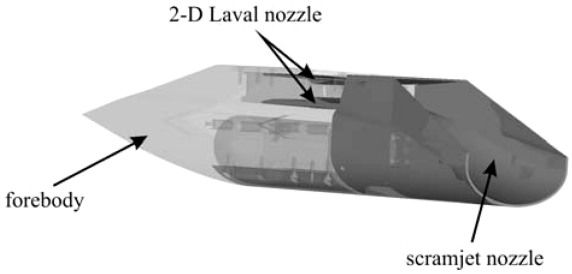

a) 3-D sketch of forebody and nozzle

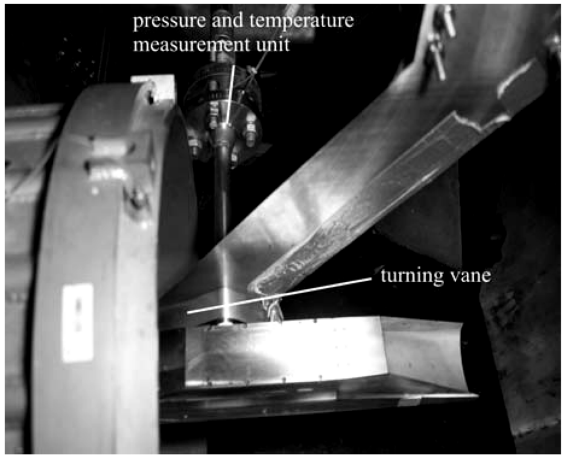

b) Model in wind tunnel

Fig. 2 Forebody and nozzle.

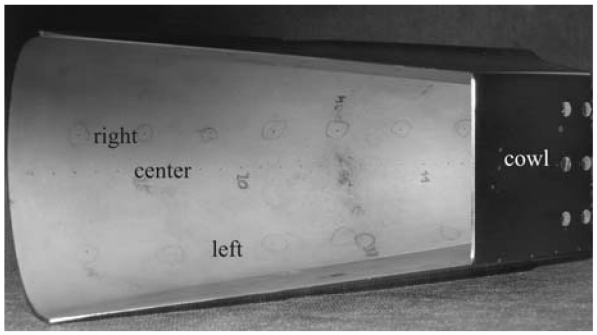

a) Photo of the nozzle

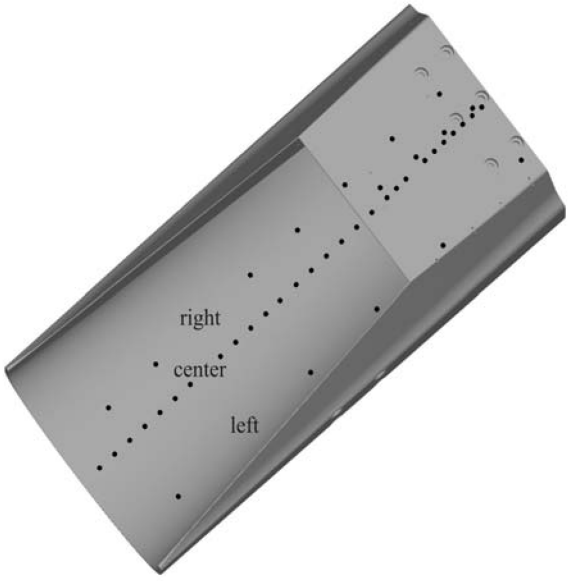

b) 3-D sketch of the nozzle

Fig. 3 Pressure orifices of the three-dimensional single expansion ramp nozzle.

placed along three different lines in the flow direction. Thirty are on the centerline, eight are displaced 15 mm to the right side, and six are displaced 30 mm to the left side of the centerline (see Fig. 3), as seen when looking down the nozzle in the flow direction. In Fig. 3b the positions of the pressure orifices are marked by the black dots. The static pressure is transmitted via pressure tubes to a Pressure System Incorporation (PSI) unit which is placed inside the forebody.

Figure 4 shows two pictures of the nozzle model installed in the wind-tunnel section. It can be seen that the model is held by a strut that is mounted to the side of the model and connected by an adapter to the model to attain a certain separation between the strut and the model. This separation prevents the shock originating from the strut leading edge from perturbing the nozzle flowfield. The strut is mounted to a model holder that can be pitched to change the angle of attack and angle of yaw of the model. During a test run the angle of attack can be varied continuously, whereas only one position for the angle of yaw can be set. The wind-tunnel flow is started as soon as the required pressure in the jet plenum has been achieved. The flow conditions, pressure and temperature, in the jet plenum are measured by the pressure and temperature measurement unit using a pitot probe and a thermocouple (Fig. 2b). The coordinate system used in this paper is shown in Fig. 4 (lower panel), the origin being marked with "0."

C. Measurement Techniques

Because the density and thus the density gradients in H2K are low, a coincident Schlieren optical setup is used to visualize the flowfield. With this technique the light beam traverses the test section twice, which leads to a higher sensitivity, but also to a slightly lower resolution. To study unsteady flow phenomena in the nozzle region, a high-speed Schlieren camera has been used. Figure 5 shows the typical coincident Schlieren optical setup of the H2K wind tunnel. The light beams emerging from the light source are concentrated by a lens onto the aperture, from where it goes to the prism. The prism sends the light beams to a mirror that leads them to another mirror while they permeate the test section. From the second mirror the light beams are sent all the way back to the camera where the density gradients can be detected due to the fact that the light beams are shifted by the density gradients.

During the experiments the jet gas total pressure $p_{0,N}$ and jet gas total temperature $T_{0,N}$ are measured with a pitot tube and a thermocouple in the plenum chamber upstream of the honeycomb. The static pressures on the single expansion ramp nozzle are measured with a PSI module with the range of 15 psi ($\sim$105 kPa). The forebody was designed to fully accommodate the PSI module, so that the pressure tubes connecting the pressure taps (orifices with diameter 0.5 mm) and the module could be kept as short as possible. For the data obtained with the PSI transducers, the error is $\pm 0.15\%$ of the full scale pressure range of the used PSI module, leading to a measurement uncertainty here of ± 1.55 mbar. Therefore, the error bars for the PSI measurement are of the size or smaller than the symbols representing their values in these figures.

III. Experimental Results

As mentioned before, the goal of this experimental study was to investigate the influence of the heat capacity ratio on the pressure distribution and on the interaction between the nozzle and external flow. For this investigation, different parameters such as the freestream Reynolds number Re_U, the nozzle pressure ratio Π, and the heat capacity ratio γ have been varied and their different effects studied. The influence of the heat capacity ratio and its effects on the nozzle flow can be seen at the different pressure distributions along the single expansion ramp and at the different interactions with the external base flow.

Because a Laval nozzle with a constant area ratio is used in these experiments, different Mach numbers and static pressures are

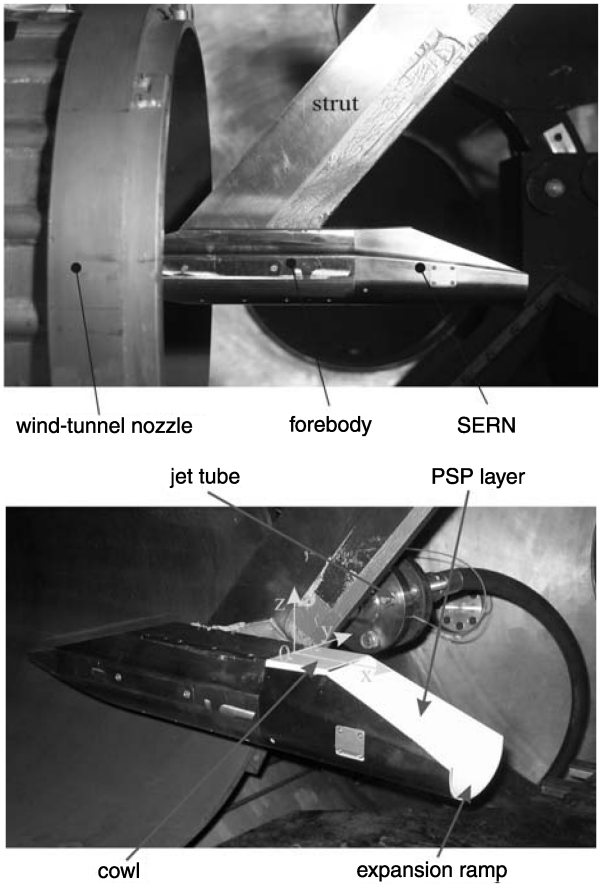

Fig. 4 Side view of the nozzle model connected to a forebody.

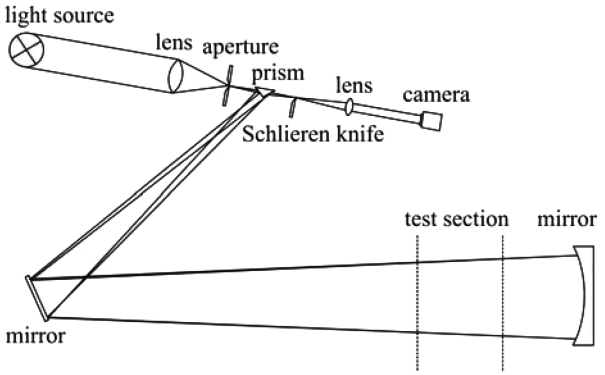

Fig. 5 Sketch of the coincident Schlieren optical setup of the H2K wind-tunnel facility.

generated at the nozzle entry and exit for the different gases. The reason for this is the different heat capacity ratio which is also illustrated by Eq. (1):

$$\frac{A^*}{A} = \frac{Ma}{\left[\frac{2}{\gamma+1}\left(1+\frac{\gamma-1}{2}Ma^2\right)\right]^{\frac{\gamma+1}{2(\gamma-1)}}} \tag{1}$$

Because of the fact that the Mach numbers, static pressures, and velocities are unequal at the entry and exit of the nozzle, proper flow parameter ratios have to be used for the investigation of the different gases. Therefore, the pressure ratios are very important and suitable parameters for simulating similar flows. Two different pressure ratio definitions were used. First the nozzle pressure ratio Π is defined as the ratio between the nozzle total pressure $p_{0.N}$ and the static pressure of the freestream p_∞. In addition, the ratio of the static pressure p_E at the nozzle exit and the static pressure p_∞ of the freestream were used. The effects of the variation of the single parameters are discussed later.

The different gases are compared for the same pressure ratio Π. In this case the nozzle total pressure is equal for air and argon if the freestream Reynolds number of the external flow is equal. It can be seen that the pressure distribution between the two gases differs distinctly (Fig. 6). In this picture the static pressure distribution along the single expansion ramp of air and argon is compared for a nozzle pressure ratio of $\Pi = 500$ and a freestream Reynolds number of $Re_U = 4 \times 10^6$. The reason for the deviation is the difference in the Mach number distribution caused by the different heat capacity ratios. According to Eq. (1) the Mach number has to be different if the area ratio remains constant and the heat capacity ratio changes. A different Mach number distribution also leads to a different static pressure distribution along the surface of the nozzle. For argon with a higher heat capacity ratio than air, a higher Mach number is obtained. For SF6 with a lower heat capacity ratio the Mach number is lower compared to air and argon. Because the Mach number and the static pressure are correlated according to Eq. (2), the static pressure distribution is correlated vice versa to the heat capacity ratio: For an increasing heat capacity ratio the static pressure decreases and for a decreasing heat capacity ratio the static pressure increases

$$\frac{p_{st}}{p_0} = \left(1+\frac{\gamma-1}{2}Ma^2\right)^{-\frac{\gamma}{\gamma-1}} \tag{2}$$

This relation explains the fact why the static pressure distribution and therefore the gross thrust for air is higher than for argon considering the heat capacity ratios of $\gamma = 1.667$ and $\gamma = 1.4$ for argon and air, respectively. The use of gases with heat capacity ratios different than air can help to simulate the influence of the heat capacity ratio of hot air, which decreases with higher temperatures.

The way in which the different heat capacity ratios affect the interaction between the nozzle and the external flow can be seen at the Schlieren photographs. In Fig. 7 the flow properties, the external and internal shock as well as the shear layer at the end of the cowl, and the definitions for the angles and pressure are depicted schematically. The picture is the base for the discussion of the Schlieren

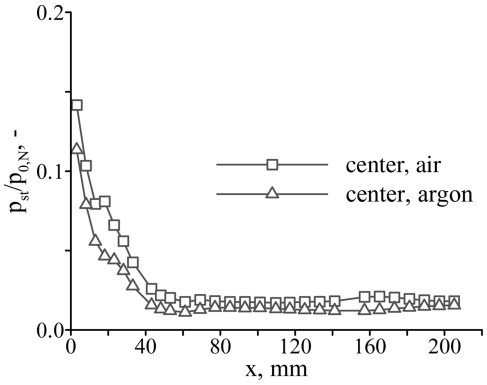

Fig. 6 Comparison of pressure distributions of air and argon along the centerline for a nozzle pressure ratio of $\Pi = 500$.

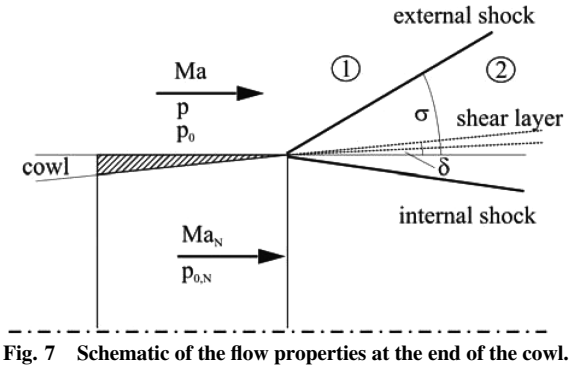

Fig. 7 Schematic of the flow properties at the end of the cowl.

photographs and shows a schematic sketch of the flow features at the end of the cowl, where nozzle flow and external flow interact. The shock wave angle is called σ, whereas the deflection angle of the flow is called δ. The conditions "1" and "2" stand for the flow conditions in front of a shock (external and internal) and behind a shock (external and internal), respectively. The pressure p_2 behind a shock is assumed to be constant over the shear layer. The angles of the external and internal shocks are just so great that the pressures adjust to each other, fulfilling the condition that the pressure is constant over the shear layer.

The visualization of the flow by the Schlieren photographs is important to estimate the influence of the heat capacity ratio of air and argon. The comparison between air and argon shows the effects on the nozzle and external flow (Figs. 8 and 9). The external flow is displaced by the nozzle flow due to the fact that the nozzle flow is underexpanded, that is, the static pressure of the nozzle flow is higher than the one of the external flow. The Schlieren photographs clearly show that the external flow is stronger displaced in the case of air than in the case of argon. The shock wave angle of the external shock is greater for air than for argon because the pressure difference between the nozzle and external flow is different for both gases: Fig. 6 proves that for smaller heat capacity ratios (air) the static pressure is greater than for higher heat capacity ratios (argon).

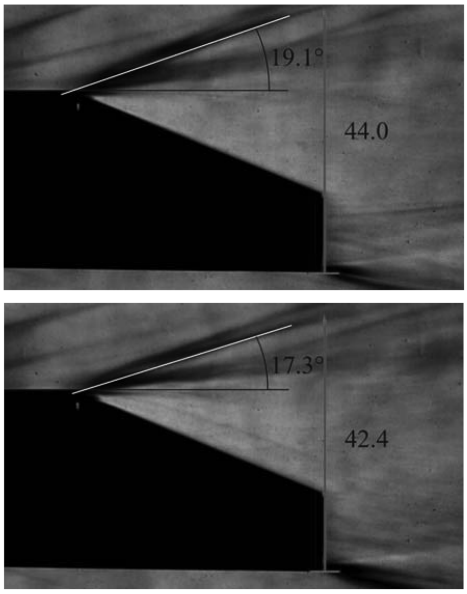

Fig. 8 Comparison of the flow topology for air (upper panel) and argon (lower panel) using Schlieren photographs taken for $\Pi = 500$ and $Re_U = 4 \times 10^6$.

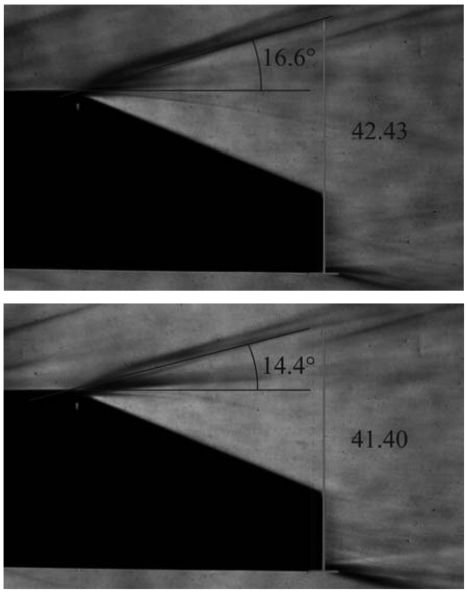

Fig. 9 Comparison of the flow topology for air (upper panel) and argon (lower panel) using Schlieren photographs taken for $\Pi = 300$ and $Re_U = 4 \times 10^6$.

That is why the expansion at the end of the cowl is stronger in the case of air than for argon and thus the displacement of the external flow is greater. This means that the nozzle flow has a greater influence on the external flow and leads to a greater deflection of the external flow. If the Mach number of the external flow is equal, a greater deflection angle δ of the flow causes a greater oblique shock wave angle σ of the external flow [see Eq. (3)]. The external shock being more oblique in the Schlieren photograph for air (Figs. 8 and 9) proves this assumption. For a known deflection angle and known Mach number the oblique shock wave angle can be determined by iteration. In the present case the oblique shock wave angle is obtained from the Schlieren photograph, and with the known Mach number Ma_1 the deflection angle can be calculated using the following relation [Eq. (3)]:

$$\delta = \arctan \frac{2 \cot \sigma (Ma_1^2 \sin^2 \sigma - 1)}{Ma_1^2 (\gamma + \cos 2\sigma) + 2} \tag{3}$$

That means that for a scramjet engine a more oblique shock wave angle causes greater pressure losses, which can be seen in Table 2 and Fig. 10. The pressure losses Δp_0 are determined by the difference between the total pressure in front of the shock p_{01} and behind the shock p_{02}. They can be calculated using the following relations (4) and (5): With the known deflection angle and oblique shock wave angle the Mach number behind the shock is computed applying Eq. (4). With Eqs. (4) and (5) the pressure loss is determined as the ratio of the total pressures p_{01} and p_{02}:

$$Ma_2 = \frac{1}{\sin(\sigma - \delta)} \cdot \frac{1}{\sqrt{\frac{\tan \sigma}{\tan(\sigma - \delta)} \cdot \frac{\gamma + 1}{2} - \frac{\gamma - 1}{2}}} \tag{4}$$

$$\frac{p_{01}}{p_{02}} = \frac{p_1}{p_2} \frac{(1 + \frac{\gamma - 1}{2} Ma_1^2)^{\frac{\gamma}{\gamma - 1}}}{(1 + \frac{\gamma - 1}{2} Ma_2^2)^{\frac{\gamma}{\gamma - 1}}} \tag{5}$$

Table 2 shows that the pressure loss in the case of air as the nozzle flow (first row) is $\Delta p_0 = 0.41$, and for argon (second row) $\Delta p_0 = 0.32$ leading to a 28% higher pressure loss for air. The base drag for air is therefore much greater than for argon and partly diminishes the advantages due to the higher static pressure along the expansion ramp and the greater gross thrust. For the design of an entire scramjet propulsion unit it has to be taken into account that with decreasing heat capacity ratio the static pressure and gross thrust increase, but at the same time the base drag and hence the net thrust decrease. This behavior is shown in Figs. 8 and 9 for two different nozzle pressure ratios. When comparing these two figures the influence of the nozzle pressure ratio can be noticed: The smaller the nozzle pressure ratio is, the less oblique the shock wave angle is and hence the smaller the base drag. For a greater heat capacity ratio (e.g., argon) a higher nozzle pressure ratio than for air can be chosen to obtain the same oblique shock wave angle. Obviously, on the one hand, the gross

Table 2 Comparison of the pressure losses Δp_0 for different oblique shock wave angles σ for air

Ma_1	σ, deg	δ, deg	Ma_2	p_{02}/p_{01}	Δp_0
7.00	19.1	12.7	4.78	0.59	0.41
7.00	17.3	10.9	5.07	0.68	0.32
7.00	16.6	10.2	5.19	0.72	0.28
7.00	14.4	7.9	5.59	0.84	0.16

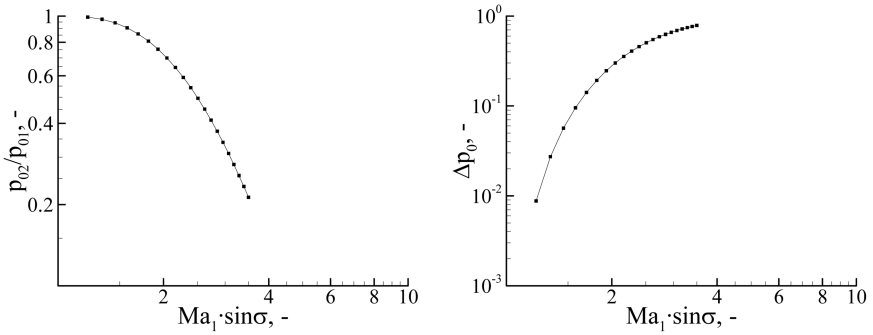

Fig. 10 Relation between shock wave angle σ and pressure ratio p_{02}/p_{01} for air (alternative: pressure loss in the right figure).

thrust is smaller than for air, but, on the other hand, the base drag is also much smaller.

For the comparison between the gas SF6 and air a similar relation is expected: Because the heat capacity ratio of sulfur hexafluoride is lower than for air, the static pressure is assumed to be higher for sulfur hexafluoride than for air in the case of the same nozzle pressure ratio and hence the same nozzle total pressure. The oblique shock wave angle, however, influenced by the interaction between the nozzle and the external flow is assumed to increase due to the stronger deflection of the external flow. The reason for the stronger deflection is that the pressure difference between the nozzle and external flow at the end of the cowl is greater for sulfur hexafluoride than for air or argon. Figure 11 shows that the static pressure is greater for sulfur hexafluoride than for air due to the lower heat capacity of $\gamma = 1.1$. The pressure distribution for the three gases depicted in this figure proves the tendencies of decreasing static pressure with increasing heat capacity ratio when comparing the pressure distribution of the three gases along the expansion ramp for a nozzle pressure ratio of $\Pi = 80$. It clearly can be seen that for the same nozzle total pressure, the static pressure distributions for the three gases differ. The reason for this is the different heat capacity ratio causing a different Mach number distribution and hence a different pressure distribution along the expansion ramp and the cowl. Therefore, a higher heat capacity ratio generates a higher static pressure distribution and thus a greater gross thrust. As can be seen at the pressure distributions for the three gases the difference between the pressure values is around 30–50% in the high pressure region at the beginning of the nozzle, where most of the thrust is generated. The momentum force at the entrance of the nozzle has to be added to the pressure force to obtain the entire gross thrust. The momentum force F is calculated by Eq. (6), where $\dot{m}$and V are the mass flow and the velocity at the entrance of the nozzle. The momentum force is almost equal for the three gases being 19.8 N for air, 20.7 N for argon, and 18.5 N for SF6 leading to a deviation of 4.5 and 6.6% for argon and SF6, respectively, from air,

$$F = \dot{m} \cdot V \tag{6}$$

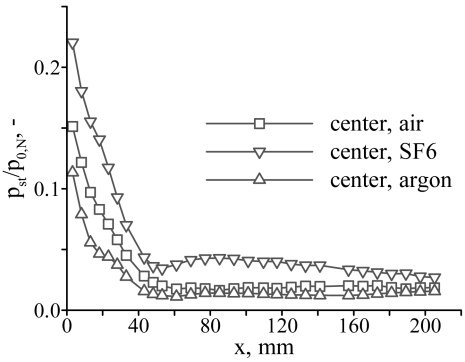

Fig. 11 Comparison of the static pressure distribution along the centerline for air, argon, and sulfur hexafluoride for a nozzle pressure ratio $\Pi = 80$ and a freestream Reynolds number $Re_U = 4 \times 10^6$.

The results for the pressure distributions confirm the results in [12,19,23], where a gas mixture of argon and freon with a heat capacity ratio of $\gamma = 1.2$ was investigated. This value of 1.2 for the heat capacity ratio is very close to the one of the combustion gas of a scramjet engine. The use of a gas or gas mixture with a heat capacity ratio very close to the one of the combustion gas helps to predict more precisely the gross thrust generated by the nozzle.

The influence on the heat capacity ratio can also clearly be seen comparing the interaction between the nozzle and external flow for the three different gases (air, argon, and SF6). Because of the previous discussion, the gas with the lowest heat capacity must theoretically have the most oblique shock wave angle σ for the same nozzle pressure ratio. In Fig. 12 it can be noticed that for sulfur hexafluoride the external shock has a shock wave angle of 15.6 deg and is the most oblique compared to air and argon. The reason is again the pressure difference at the end of the cowl being greater in the case of sulfur hexafluoride than for air and argon, which can be seen in Fig. 12.

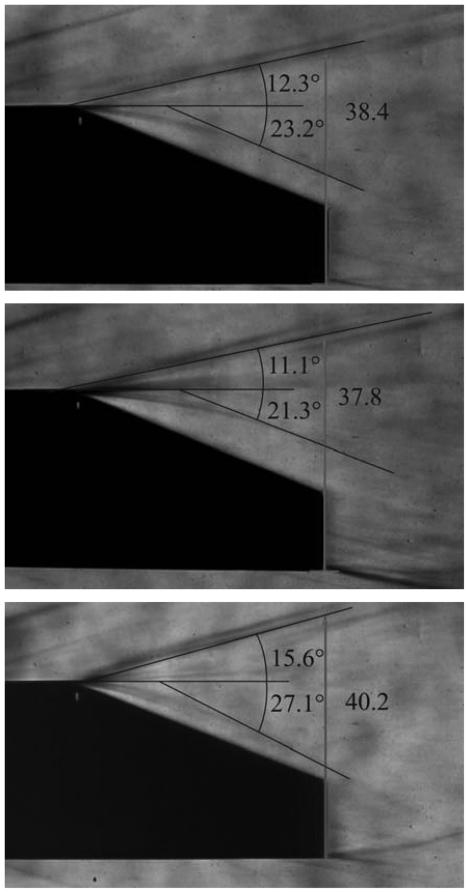

Fig. 12 Comparison of the flow topology for air (top panel), argon (middle panel), and SF6 (bottom panel) using Schlieren photographs for $\Pi = 80$ and $Re_U = 4 \times 10^6$.

Table 3 Comparison of oblique shock wave angle and Mach numbers at the end of the cowl for air, SF6, and argon

Gas	γ	R	Ma_N	$p_{0,N}$	σ, deg	δ, deg	p_2/p_N
Air	1.4	287	3.17	0.22	20.5	3.1	1.28
SF6	1.1	56	2.61	0.22	23.6	1.7	1.1
Argon	1.667	218	3.80	0.22	19.4	5.1	1.74

As shown in Table 3 for all test cases due to the oblique shock in the external flow the pressure behind the shock p_2 becomes higher than the static pressure of the nozzle flow p_N at the end of the cowl. In Table 3 the different Mach numbers at the end of the cowl caused by the different heat capacity ratios can also be seen. The different Mach numbers lead to different pressure differences, strengths of expansion, deflection of the external flow, oblique shock wave angles, and base drags.

In this case the nozzle flow is called overexpanded causing a very oblique internal shock wave. For sulfur hexafluoride, this internal shock is the most oblique due to the low heat capacity ratio; the shock angle is 27.1 deg compared to 23.2 for air and 21.3 deg for argon as can be seen in Fig. 12.

Comparing the three gases with different heat capacity ratios it can be stated that for the gas with the lowest heat capacity ratio (SF6) the highest gross thrust is obtained, but at the same time the greatest base drag is generated by the interaction between internal and external flow. Therefore, a compromise has to be found between a possibly high static pressure distribution leading to a high gross thrust and a possibly low base drag when designing an entire scramjet propulsion unit.

Furthermore, by using gases with different heat capacity ratios, the ratio of the static pressures at the end of the expansion ramp has been investigated besides the nozzle pressure ratio. Keeping the ratio of the static pressures at the nozzle exit equal for the different gases, the same effects such as pressure distribution and interaction between the nozzle and external flow have been experimentally studied. Because of the different Mach number distribution the equivalent ratio of the static pressures causes different nozzle pressure ratios Π and hence different nozzle total pressures $p_{0,N}$. To realize the same ratio of the static pressures at the end of the nozzle, a nozzle pressure ratio of $\Pi = 625$ for air and $\Pi = 1230$ for argon has to be set. Figure 13 shows the resulting pressure coefficient distribution along the centerline of the expansion ramp for two different freestream Reynolds numbers; the two graphs for air and argon agree very well, especially from a downstream position of $x = 50$ mm. This means that the static pressure distribution and the gross thrust are nearly equal. This leads to the conclusion that the pressure distribution of gases with different heat capacity ratios can be suitably simulated by keeping the ratio of the static pressures at the nozzle exit equal. One explanation for this observation can be that for both cases the flow expands to the same pressure level at the nozzle exit and therefore the pressure level adjusts to the same values along the entire nozzle. It also justifies the assumption that the ratio of the static pressures at the nozzle exit is an important parameter for the simulation of nozzle flows with different heat capacity ratios. For the unknown pressure, distribution for a certain gas can be obtained from a known pressure distribution for a different heat capacity ratio. In the case of a scramjet engine the nozzle gas has a heat capacity ratio below 1.4 (about 1.25) after the combustion. If the heat capacity ratio of the combustion gas is known, the static pressure distribution for this gas can be computed from a static pressure distribution for a gas with a different heat capacity ratio by adjusting the nozzle pressure ratio.

The equivalent Schlieren photographs for the freestream Reynolds number $Re_U = 8 \times 10^6$ are depicted in Fig. 14. The pictures show that the shock wave angle for argon is much greater than for air. The reason for this is that the nozzle total pressure and thus the static pressure are higher at the end of the cowl in the case of argon: Therefore, the nozzle flow expansion is stronger leading to a greater deflection of the external flow and a greater shock wave angle of the external shock. The greater shock wave angle causes a greater base drag which has to be taken into account in designing a scramjet propulsion unit.

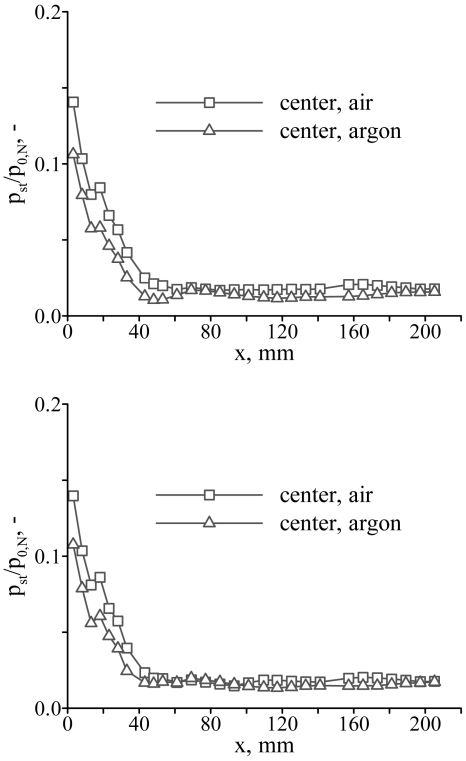

Fig. 13 Pressure distribution of air and argon along the centerline for equal static pressures at the nozzle exit for two different freestream Reynolds numbers $Re_U = 4 \times 10^6$ (top panel) and $Re_U = 8 \times 10^6$ (bottom panel): air $\Pi = 625$; argon $\Pi = 1230$.

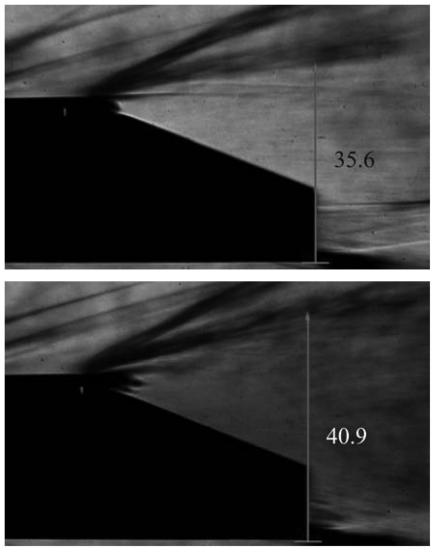

Fig. 14 Comparison of the flow topology for air (top panel) and argon (bottom panel) using Schlieren photographs for a freestream Reynolds number $Re_U = 8 \times 10^6$ for $\Pi = 625$ (air) and $\Pi = 1230$ (argon).

The effects of a parameter variation of the nozzle pressure ratio Π can be seen in Fig. 15. The nozzle pressure ratio is varied from $\Pi = 190$ to $\Pi = 700$, while air is used as the jet fluid. The nozzle total pressure $p_{0,N}$ increases with higher nozzle pressure ratios, because the freestream Reynolds number and hence the static pressure of the stream are kept constant. The static pressure along the surface of the single expansion ramp increases because the area ratio and thus the Mach number distribution remain constant under the

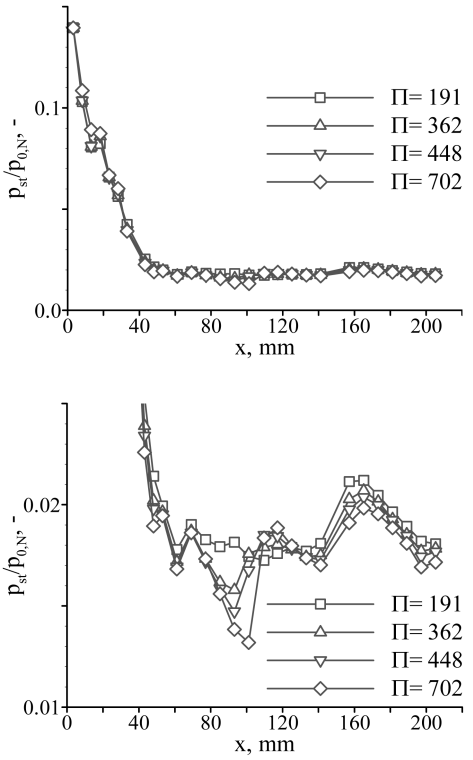

Fig. 15 Normalized pressure distribution along the centerline for different nozzle pressure ratios Π and for $Re_U = 8 \times 10^6$; top panel: all data points; bottom panel: magnified region.

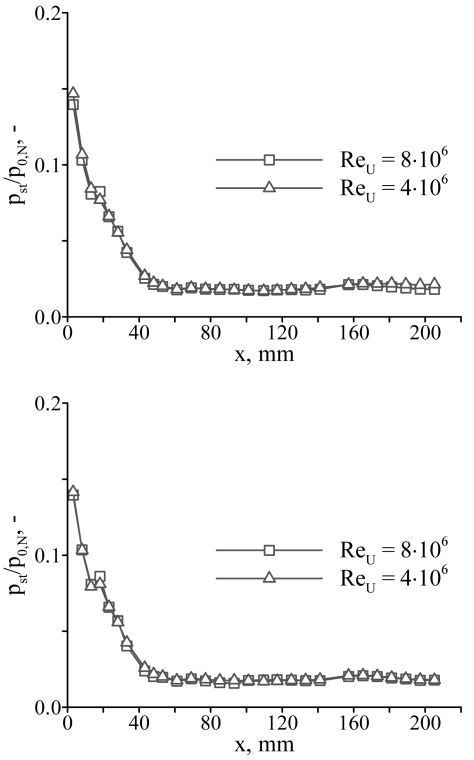

Fig. 16 Pressure distribution along the centerline for different freestream Reynolds numbers; top panel: Π = 250; bottom panel: Π = 500.

condition of a constant heat capacity ratio. If the static pressure is normalized by the nozzle total pressure as is done in the present work, it can be seen that the pressure distributions are almost equal. This implies that the qualitative distribution of the static pressure is independent from the nozzle pressure ratio. Having a closer look at the pressure distribution it can be recognized, however, that the pressure distributions at the streamwise positions between $x =$ 70 mm and 110 mm as well as between $x = 140$ mm and 170 mm are influenced by the nozzle pressure ratio.

It can be observed that with increasing nozzle pressure ratio the pressure decreases in the aforementioned regions. Moreover, in the magnified picture the wavy pressure distribution is noticeable, that is, the pressure increases and decreases along the expansion ramp. This unexpected behavior is more significant for higher nozzle pressure ratios. It implies certain perturbations along the centerline, because a constant pressure decrease is usually expected. By normalizing the pressure distribution the influence of the nozzle pressure ratio in certain regions is revealed, but not along the entire centerline (Fig. 15). It is concluded that it is mainly the geometry of the expansion ramp which affects the pressure distribution and its wavy behavior. This influence increases with increasing nozzle pressure ratio. Further experimental studies with additional measurement techniques were performed to gain more information and explain this phenomenon [24]. These experimental studies showed that certain perturbations emerging from the internal expansion and also the nozzle geometry caused these pressure distributions.

The influence of the freestream Reynolds number Re_U on the nozzle flow properties has also been investigated. For a fixed nozzle pressure ratio of $\Pi = 500$, an experimental study for a Reynolds number range from 4×10^6 to 8×10^6 was performed. As shown in Fig. 16, the differences in the static pressure distribution for two different nozzle pressure ratios are very small. The influence of the freestream Reynolds number and the external flow on the pressure coefficient distribution and the gross thrust are small. Therefore, it can be concluded that the nozzle pressure ratio is a good parameter for the prediction of the pressure coefficient distribution as well as the gross thrust for single expansion ramp nozzles independent of the external flow conditions. For this reason the influence of the

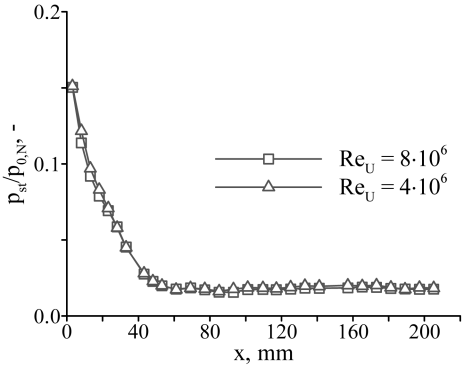

Fig. 17 Pressure distribution along the centerline for different freestream Reynolds numbers and Π = 80.

freestream Reynolds number and the external flow on the static pressure distribution of the nozzle flow and thus on the gross thrust are rather negligible in the investigated region. The external flow, however, has a great influence on the base drag of the scramjet engine and hence on the net thrust of the propulsion unit.

Even for the overexpanded condition of the nozzle, the influence of the Reynolds number is very small. It has been noticed that for this nozzle geometry the transition from an underexpanded nozzle to an overexpanded one occurs at a nozzle pressure ratio of around $\Pi = 150$. Experimental data at a nozzle pressure ratio of $\Pi = 80$ show no significant differences except the parallel displacement of the graph (Fig. 17): The graphs of the pressure distribution for the two different freestream Reynolds numbers are almost identical.

IV. Conclusions

An experimental study has been conducted with a generic nozzle/afterbody model to characterize the flowfield created by the interaction of a single expansion ramp nozzle and the external flow. To make a distinction between the influence of the specific heat ratio

and viscosity change with increasing temperature on the nozzle flow properties and nozzle performance as well as the interaction of the internal nozzle flow with the external flow, three different exhaust gases were used. It has been noticed that several parameters of the external and nozzle flow influence the pressure distribution and thereby the gross thrust of the presented single expansion ramp nozzle. Moreover, these flow parameters affect the interactions between the nozzle flow and the external flow, which lead to changes in the base drag of the single expansion ramp nozzle.

The heat capacity ratio affects the pressure coefficient distribution in such a way that the increasing heat capacity ratio leads to decreasing pressure and vice versa. The experiments with different gases were also performed to distinguish between the influence of heat capacity ratio and the nozzle total temperature. Previous studies where the influence of the nozzle total temperature was studied in a range from 300 to 800 K [25] showed that the influence of the heat capacity ratio on the pressure distribution is much stronger, whereas the influence of the nozzle total temperature on the pressure distribution is almost negligible in the investigated temperature region. At selected test conditions the heat capacity ratio has a more dominant influence on the gross thrust.

The external flow is also affected by the heat capacity ratio of the nozzle flow. An increasing heat capacity ratio leads to weak external oblique shocks reducing the base drag. A decreasing heat capacity ratio causes a lower Mach number and a higher static pressure at the end of the cowl leading to stronger external oblique shocks. Because of the fact that stronger oblique shocks cause higher pressure losses the base drag increases for lower heat capacity ratios. This fact diminishes the advantage of higher gross thrust for lower heat capacity ratios. These observations have to be taken into account for the design process of the scramjet engine. Further investigations using lower heat capacity ratios are necessary to have a complete figure of the dependency of the interaction between internal and external flows. To investigate the viscous effects at high gas temperature and distinguish this influence from the influence of the heat capacity ratio, experiments with a hot nozzle flow with total temperatures beyond 2000 K have to be carried out.

Furthermore, the influence of the nozzle pressure ratio and the freestream Reynolds number has been investigated. The nozzle pressure ratio has the main influence on the gross thrust, but it also influences the interaction between the nozzle and the external flow in a negative way: A higher nozzle pressure ratio generates a higher gross thrust, but it also causes a greater base drag. The data of the pressure measurements and the Schlieren photographs showed that the influence of the Reynolds number variation by a factor of about 2 on the pressure coefficient is rather negligible.

Acknowledgments

The financial support for this work by the German National Research Council within the graduate college "Aerothermodynamic Design of a Scramjet Propulsion System for Future Space Transportation" and by the DLR, Cologne, is acknowledged.

References

[1] Walther, R., "Scramjet-Propulsion: alte Herausforderung im neuen Jahrhundert?," *Jahrbuch 2003 der Deutschen Gesellschaft für Luft- und Raumfahrt—Lilientahl-Obert, e. V.*, DGLR, München, 2003, pp. 755–764.

[2] Curran, E. T., and Murthy, S. N. B., *Scramjet Propulsion*, Vol. 189, AIAA, Reston, VA, 2000.

[3] Fry, R. S., "A Century of Ramjet Propulsion Technology Evolution," *Journal of Propulsion and Power*, Vol. 20, No. 1, 2004, pp. 27–58. doi:10.2514/1.9178

[4] Spaid, F. W., and Keener, E. R., "Hypersonic Nozzle/Afterbody CFD Code Validation Part 1: Experimental Measurements," AIAA Paper 93-0607, 1993.

[5] Spaid, F. W., Keener, E. R., and Hui, F. C. L., "Experimental Results for a Hypersonic Nozzle/Afterbody Flow Field," NASA Ames Research Center, NASA TM-4638, 1995.

[6] Gruhn, P., Henckels, A., and Sieberger, G., "Improvement of the SERN Nozzle Performance by Aerodynamic Flap Design," *Aerospace Science and Technology*, Vol. 6, No. 6, 2002, pp. 395–405. doi:10.1016/S1270-9638(02)01177-X

[7] Flandro, G. A., Roach, R. L., and Buschek, H., "Dynamic Interactions Between Hypersonic Vehicle Aerodynamics and Propulsion System Performance," NASA Center for AeroSpace Information (CASI), NASA-CR-190638, 1992.

[8] Edwards, T. A., "The Effect of Exhaust Plume/Afterbody Interaction on Installed Scramjet Performance," NASA Center for AeroSpace Information (CASI), NASA-TM-101033, 1988.

[9] Baysal, O., "Flow Analysis and Design Optimization Methods for Nozzle Afterbody of a Hypersonic Vehicle," NASA Center for AeroSpace Information (CASI), NASA-CR-4431, 1991.

[10] Ebrahimi, H. B., "An Efficient Two-Dimensional Engineering Design Code for Scramjet Combustor, Nozzle, and Plume Analysis," AIAA Paper 91-0416, 1991.

[11] Ishiguro, T., Takaki, R., Mitani, T., and Hiraiwa, T., "Three-Dimensional Analysis of Scramjet Nozzle Flows," *AIAA/DGLR Fifth International Aerospace Planes and Hypersonics Technologies Conference*, AIAA, Washington, D.C., 1993.

[12] Tatum, K., Monta, W., Witte, D., and Walters, R., "Analysis of Generic Scramjet External Nozzle Flowfields Employing Simulant Gases," AIAA Paper 90-5242, 1990.

[13] Keener, E. R., "Experimental Research of the Aerodynamics of Nozzles and Plumes at Hypersonic Speeds," NASA Center for AeroSpace Information (CASI), NASA-CR-187316, 1992.

[14] Carboni, J. D., Shyne, R. J., Leavitt, L. D., Taylor, J. G., and Lamb, M., "Supersonic Investigation of Two Dimensional Hypersonic Exhaust Nozzles," NASA Center for AeroSpace Information (CASI), NASA-TM-105687, 1992.

[15] Lindblad, I. A. A., Grönland, T. A., Cambier, J.-L., Wallin, S., Behrens, T. M., Sacher, P., and Netterfield, M., "A Study of Hypersonic Afterbody Flowfields," AIAA Paper 97-2289, 1997.

[16] Tomioka, S., Hiraiwa, T., and Mitani, T., "A Study on Boundary Layer in a Scramjet Nozzle Operating Under High Enthalpy Conditions," *30th AIAA/ASME/SAE/ASEE Joint Propulsion Conference*, AIAA, Washington, D.C., 1994.

[17] Weigand, B., Gaisbauer, U., Reinhartz, B., Kau, H.-P., and Schröder, W., "Aero-Thermodynamische Auslegung eines Scramjets—Antriebssystems für Zukünftige Raumtransportsysteme," DGLR-Tagung, 2006.

[18] Mitani, T., Kanda, T., Hiraiwa, T., Igarashi, Y., and Nakahashi, K., "Drags in Scramjet Engine Testing: Experimental and Computational Fluid Dynamics Studies," *Journal of Propulsion and Power*, Vol. 15, No. 4, 1999, pp. 578–583. doi:10.2514/2.5466

[19] Pittman, J. L., "A Mach 6 External Nozzle Experiment with Argon-Freon Simulation," *Aerospace Technology Conference and Exposition*, Society of Automotive Engineers, Warrendale, PA, 1989.

[20] Hirschen, C., Gruhn, P., and Gülhan, A., "Influence of Heat Capacity Ratio on the Interaction between External Flow and Nozzle Flow of a Scramjet," AIAA Paper 2006-8095, 2006.

[21] Niezgodka, F.-J., "Der Hyperschallwindkanal H2K des DLR in Köln Porz (Stand 2000)," ISSN 1434-8462, 2001.

[22] Novelli, P., and Koschel, W., "Japhar: A Joint Onera—DLR—Project on High Speed Airbreathing Propulsion," ISABE Paper 99-7091, 1999.

[23] Tatum, K. E., and Huebner, L. D., "Exhaust Gas Modeling Effects on Hypersonic Powered Simulation at Mach 10," AIAA Paper 1995-6068, 1995.

[24] Hirschen, C., Gülhan, A., Beck, W. H., and Henne, U., "Experimental Study of a Scramjet Nozzle Flow Using the Pressure Sensitive Paint Method," *Journal of Propulsion and Power*, Vol. 24, No. 4, 2008, pp. 662–672. doi:10.2514/1.34626

[25] Hirschen, C., and Gülhan, A., "Experimental Study of the Single Expansion Ramp Nozzle Flow Properties and its Interaction with the External Flow," *1st CEAS European Air and Space Conference*, DGLR, 367, Berlin, 2007.

R. Bowersox
Associate Editor